

Supporting Information

Synergistic photoluminescence enhancement in conjugated polymer-di-ureasil organic-inorganic composites

Niamh Willis-Fox,^a Ana-Teresa Marques,^{b,c} Jochen Arlt,^d Ullrich Scherf,^b Luís D. Carlos,^e
Hugh D. Burrows^c and Rachel C. Evans^{a*}

^a School of Chemistry and CRANN, Trinity College, The University of Dublin, Dublin 2, Ireland. E-mail: raevans@tcd.ie

^b Makromolekulare Chemie, Bergische Universität Wuppertal, 42097 Wuppertal, Germany.

^c Departamento de Química, Universidade de Coimbra, 3004–535 Coimbra, Portugal.

^d Collaborative Optical Spectroscopy, Micromanipulation and Imaging Centre (COSMIC) and SUPA, King's Buildings, School of Physics, King's Buildings, University of Edinburgh, EH9 3JZ, U.K.

^e Departamento de Física and CICECO, Universidade de Aveiro, 3810–193 Aveiro, Portugal.

Table of Contents

1. Materials
2. Synthesis of conjugated polyelectrolyte (CPE)-di-ureasils
3. Instrumentation
4. Determination of photoluminescence quantum yields
5. Supporting experimental data
 - 5.1 Solvent permeation studies
 - 5.2 CPE release studies
 - 5.3 Powder X-ray diffraction
 - 5.4 Solid-state nuclear magnetic resonance (NMR)
 - 5.5 Fourier transform infrared (FTIR) spectroscopy
 - 5.6 Steady-state photoluminescence studies
 - 5.7 Picosecond time-correlated single photon counting (TC-SPC) studies
6. References

1. Materials

Poly(propylene glycol)-block-poly(ethylene glycol)-block-poly(propylene glycol) *bis* (2-aminopropyl ether) (Jeffamine ED-600), 3-isocyanatopropyltriethoxysilane (ICPTES), ethanol (HPLC grade), hydrochloric acid (37% Puriss), potassium bromide (FTIR grade), acetonitrile (HPLC grade) and 1,4-dioxane (HPLC grade) were purchased from Sigma Aldrich and were used as received. Tetrahydrofuran (THF) (99.9%) was obtained from Fischer Scientific and used as received. Poly[9,9-bis(4-sulfonylbutoxyphenyl) fluorene-2,7-diyl-*alt*-1,4-phenylene] (PBS-PFP) and poly{9,9-bis[6-(*N*, *N*, *N*-trimethylammonium)hexyl]fluorene-2,7-diyl-*alt*-1,4-phenylene} (PFP-HTMA), both with a M_n 6500 g mol⁻¹ by gel permeation chromatography (~740 g mol⁻¹ repeat units (r.u.) for PBS-PFP and ~776 g mol⁻¹ (r.u.) for PFP-HTMA), were synthesised as previously reported.¹⁻

3

2. Synthesis of CPE-di-ureasils

CPE-di-ureasil composites were prepared *via* two different methods: direct insertion and solvent permeation. Both methods involve the preparation of a di-ureapropyltriethoxysilane (d-UPTES) precursor solution, which has been described in detail elsewhere.⁴⁻⁶ In brief, Jeffamine ED-600 (1 ml, 1.75 mmol) was dissolved in THF (5 ml), to which 3-isocyanatopropyltriethoxysilane (ICPTES) (0.9 ml, 3.0 mmol) was added under stirring. This mixture was refluxed at 70 °C for 24 hr to prepare the d-UPTES precursor solution. The undoped di-ureasil is obtained by addition of ethanol (0.409 ml, 7 mmol), HCl (0.5 M, 0.040 ml) and H₂O (0.095 ml, 5.3 mmol) to the d-UPTES solution, which triggers the acid-catalysed sol-gel reaction. This corresponds to a ratio of 1 ICPTES: 2.3 EtOH: 1.8 H₂O: 0.006 HCl molar equivalents. The solution was stirred for 5 min before being poured into a polyurethane mould which was then covered with Parafilm. After 24 hr, the Parafilm was pierced to encourage slow evaporation of the solvent. The samples were then placed in the oven at 40 °C for 48 hr to complete the drying process which produced free-standing, transparent monoliths.

In the direct insertion method, a fixed volume of CPE solution was added to the d-UPTES precursor described above, prior to the addition of the gelation agents. The volume of the CPE solution was varied to produce CPE-di-ureasils with the doped wt% described in Table 1. In the solvent permeation method, preformed blank di-ureasils were placed in a CPE

solution of fixed volume (4 ml) and known concentration, upon which the hybrid swells taking up the CPE solution in which it is immersed. The concentrations of stock CPE solution used are outlined in Table 1. Following immersion for 200 min, the samples were removed and allowed to dry for 24 hr, after which the samples contracted back to their initial size and form.

3. Instrumentation

Fourier Transform Infrared (FTIR) spectra were recorded on a Perkin-Elmer spectrum 100 FTIR spectrometer at room temperature. FTIR spectra were collected over a range of 4000-400 cm^{-1} by averaging 64 scans at a resolution of 4 cm^{-1} . The samples (2 mg) were finely ground and mixed with potassium bromide (175 mg) and pressed into pellets. To evaluate the contributions to the Amide I band spectral deconvolution using Gaussian band fitting was carried out using Origin 8.0® in the region of 1610-1770 cm^{-1} .

Powder X-ray diffraction (PXRD) patterns were recorded using a Siemens D500 diffractometer. The samples were exposed to the Cu K_{α} radiation ($\lambda = 1.54 \text{ \AA}$) at room temperature in the range 5-70° (2θ).

Solid-state ^{29}Si and ^{13}C cross polarised (CP) and directly polarised (DP) nuclear magnetic resonance (NMR) spectroscopy were performed at ambient temperature on a Varian VNMRS instrument operating at 79.435 MHz for ^{29}Si and 100.56 MHz for ^{13}C . Spectra were recorded against an external tetramethyl silane (TMS) standard with magic angle spinning (MAS) at a spinning rate of 4300-5000 Hz. The ^{13}C CP spectra were obtained as single contact experiments with a contact time of 5 ms and a recycle delay of 1.0 s (700 repetitions).

Thermogravimetric analysis was performed using a Perkin Elmer Pyris 1 TGA thermogravimetric analyser in the range 30-900 °C in an air atmosphere using *ca.* 2-5 mg sample, at a heating rate of 10 °C min^{-1} in a ceramic crucible. The instrument was calibrated against In and Ni standards in an air atmosphere.

Steady-state PL spectroscopy was performed on a Fluorolog-3 spectrophotometer (Horiba Jobin Yvon), using the front-face configuration for solid state samples. Emission and excitation spectra were corrected for the wavelength response of the system and the intensity of the lamp profile over the excitation range, respectively, using correction factors supplied by the manufacturer. The emission and excitation slit width were fixed at 2.5 nm. PL quantum yields were measured using an F-3018 integrating sphere accessory. The values

reported are the mean of three repeat measurements. The method is accurate to within 10%.

Photostability studies were carried out on CPE-di-ureasil samples and a thin film of pure PBS-PFP. The CPE thin film was prepared by spin-coating PBS-PFP (10 mg/ml in 1,4-dioxane/THF 20/80 v/v) onto a glass slide at a rate of 2000 rpm. Photostability experiments were performed using the same experimental configuration used for PL measurements. Samples were irradiated using a Xe arc lamp (450 W) for 2 h at an excitation wavelength of 370 nm. The integrated emission intensity of the sample was measured at selected irradiation intervals. The irradiation power of the source was quantified using a photodiode (Newport, 818-UV-L detector) with an attached OD3 attenuator with a diameter of 50 μm , coupled to a Keithly 2401 Sourcemeter in two probe mode with Tracer2 software, yielding an irradiance value of 266.4 W/m^2 .

Fluorescence decays were measured using the picosecond time-correlated single photon counting (TCSPC) method at the Collaborative Optical Spectroscopy, Micromanipulation and Imaging Centre (COSMIC), University of Edinburgh, U.K. The excitation source was the second harmonic of the pulse-picked output of a Ti-Sapphire femtosecond laser system (Coherent, 10 W Verdi and Mira Ti-Sapphire), consisting of pulses of ~ 200 fs at 4.75 MHz repetition rate. Fluorescence decays were measured using an Edinburgh Instruments spectrometer equipped with TCC900 photon counting electronics. The instrument response of the system was ~ 50 ps FWHM. Fluorescence decay curves were analysed using a standard iterative reconvolution method, assuming a multiexponential decay function. For wavelength scan experiments, the sample DI-PBS-1.0 was excited at 365 nm and the fluorescence decays were recorded with increasing emission wavelength ($\lambda_{\text{em}}=400, 410, 420, 430, 440, 450, 460, 470, 480, 490$ and 500 nm). Reconvolution and data-fitting was performed as an individual fit to each decay using DAS6 software (HORIBA). For the concentration studies, samples were excited at 365 nm and the fluorescence decays were recorded at emission wavelengths of 420 and 500 nm. Reconvolution and fitting of the fluorescence decays were carried out using Globals WE[®] software package.⁷ Global analysis was carried out on each sample on the decays collected at an emission wavelength of 420 and 500 nm linking the component at ~ 0.3 ns which appears both in the decays at 420 and 500 nm. The quality of fit was judged on the basis of the reduced chi-square statistic, χ^2 , and the randomness of residuals.

Confocal microscopy was performed using a Carl Zeiss LSM 700 confocal laser scanning system on an Axio Observer.Z1 inverted microscope stand with an excitation wavelength of 405 nm.

4. Determination of photoluminescence quantum yields (PLQY)

Photoluminescence from solid-state samples is typically emitted in a non-uniform spatial pattern due to the anisotropic distribution of chromophores and corresponding emission dipole moments.⁸ PLQY of solids and thin films are thus usually determined using an integrating sphere, which eliminates this challenge to some extent.^{8, 9} For optically thick samples such as the CPE-di-ureasils described here, waveguiding of the emitted light and/or reabsorption of the emitted photons may also lead to errors in the measured PLQY. To account for these factors, absolute PLQY measurements were first performed following the procedure reported by de Mello *et al.*⁹ The observed PLQY values (PLQY_{obs}) were subsequently corrected for self-absorption using the method described by Ahn *et al.*⁸ This approach takes into account both the initial emission and subsequent absorption and remission processes to determine the true PLQY. It is assumed that at the red-edge of the emission spectrum, where sample absorption is negligible, emission/reabsorption/remission occurs but does not lead to spectral reshaping. The long wavelength emission is thus described by:

$$F'(\lambda) = \frac{F(\lambda)}{1-\alpha(PLQY)} = \alpha F(\lambda) \quad (1)$$

where $F(\lambda)$ is the photoluminescence spectrum in photons per wavelength, normalised to $\int_0^\infty F(\lambda) d\lambda = 1$. The factor α represents an empirical factor that scales the true spectrum $F(\lambda)$ (obtained by measuring the photoluminescence for a sample whose spectrum is not distorted by self-absorption) to an enhanced spectrum $F'(\lambda)$ whose red-edge is matched to that of the observed photoluminescence spectrum $F_{obs}(\lambda)$.

The probability of self-absorption of an emitted photon, α , is determined from:

$$\frac{\int_0^\infty F_{obs}(\lambda) d\lambda}{\int_0^\infty F'(\lambda) d\lambda} = 1 - \alpha \quad (2)$$

which enables determination of the true photoluminescence quantum yield (PLQY) from:

$$PLQY = \frac{PLQY_{obs}}{1-\alpha+\alpha(PLQY_{obs})} \quad (3)$$

Ideally, the true photoluminescence spectrum ($F(\lambda)$) is obtained by measuring a dilute solution of the lumophore where self-absorption is absent. However, in CPE-di-ureasil systems, both the CPE and the di-ureasil are photoluminescent and no solution state

equivalent exists. To overcome this, the true spectrum for each series is taken to be that of the lowest wt% sample measured in the front-face configuration (not in the integrating sphere).

In fact, self-absorption effects are minimal for these materials. This is illustrated in Figure S1 for DI-PBS-2.0 as an example. Good agreement between the solution-phase photoluminescence spectrum of PBS-PFP and the front-face photoluminescence spectrum of DI-PBS-2.0 is obtained, illustrating that utilisation of the front-face measurement to represent the “true” emission spectrum is reasonable. Only a minor correction for re-absorption effects are required for the corresponding measurement in the integrating sphere, which results in a negligible change in the PLQY (Figure S2).

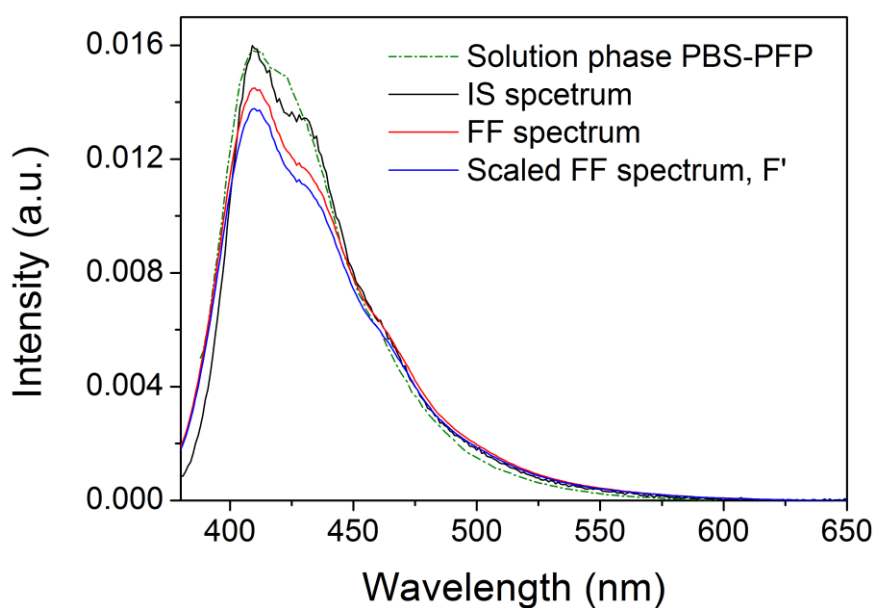


Figure S1. Area-normalised solution phase emission spectrum for PBS-PFP in 25:75 % v/v 1,4-dioxane/water (green dash line), the area-normalised integrating sphere (IS) photoluminescence spectrum ($F_{\text{obs}}(\lambda)$) (black line), the area-normalised front-face (FF) photoluminescence spectrum ($F(\lambda)$) (red line) and the scaled, unattenuated photoluminescence spectrum ($F'(\lambda)$) for DI-PBS-2.0. The scale factor, α , is adjusted so that $F'(\lambda)$ matches $F_{\text{obs}}(\lambda)$ at $\lambda_{\text{em}} = 500$ nm and longer.

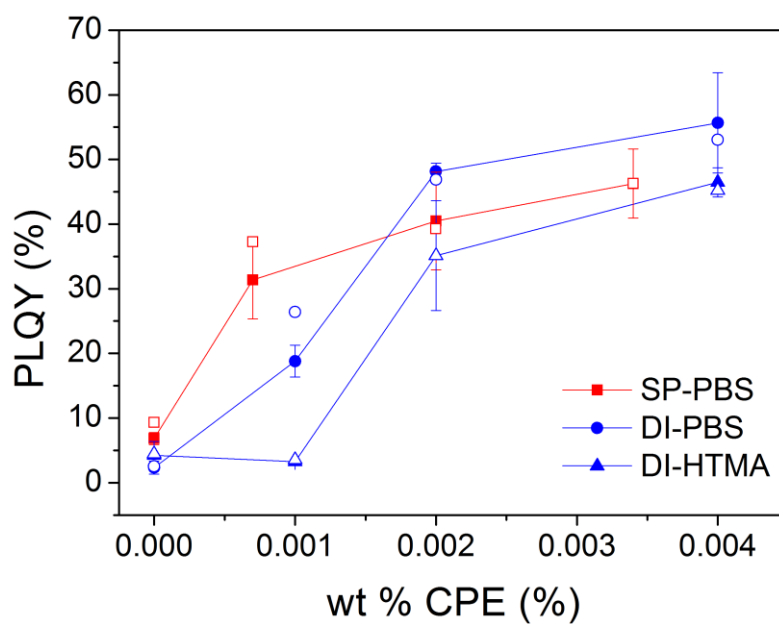


Figure S2. Measured photoluminescence quantum yield ($\lambda_{\text{ex}}=370$ nm) for SP-PBS- x (closed red squares), DI-PBS- x (closed blue circles) and DI-HTMA- x (closed blue triangles). The open symbols represent the corresponding PLQY values corrected for re-absorption/re-emission. The solid lines serve solely to guide the eye.

5. Supporting experimental data

5.1 Solvent permeation studies

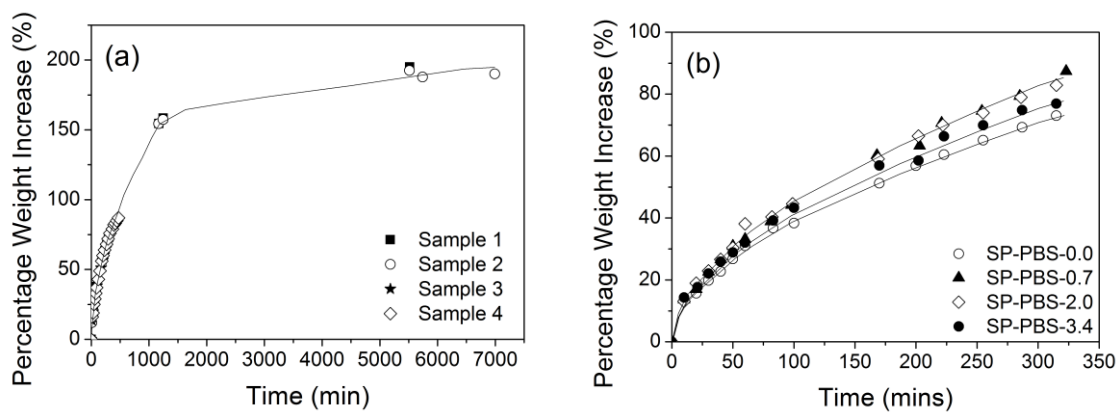


Figure S3. (a) Percentage weight increase for di-ureasil samples as a function of immersion time for the *Solvent Permeation* method in 1, 4 dioxane/H₂O (25:75% v/v); sample 1 - closed squares, sample 2 - open circles, sample 3 - closed stars, sample 4 - open diamonds. (b) Percentage weight increase for di-ureasil samples as a function of immersion time in PBS-PFP solution (25:75 % v/v 1,4-dioxane/water); SP-PBS-0.0 - open circles, SP-PBS-0.7 - closed triangles, SP-PBS-2.0 - open diamonds, SP-PBS-3.4 - closed circles – SP-PBS-3.4. The solid lines serve only to guide the eye.

5.2 CPE release studies

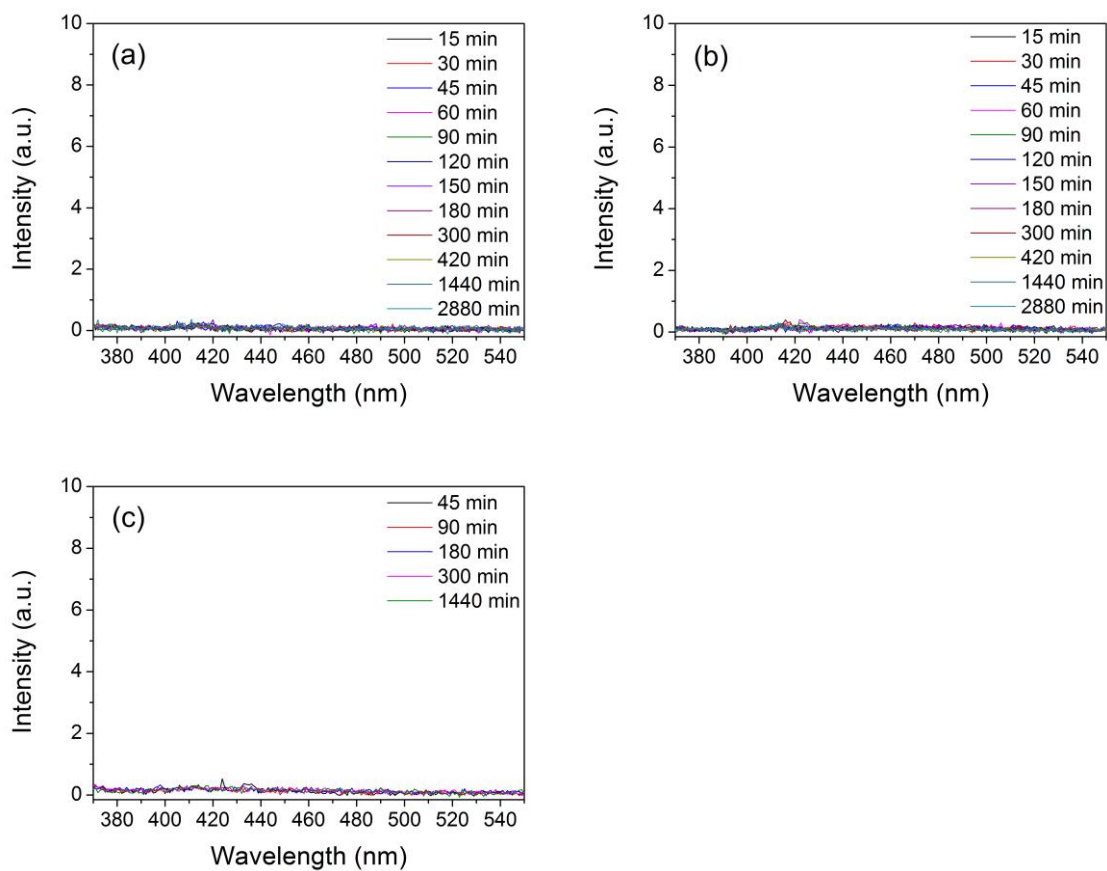


Figure S4. Photoluminescence spectra of the immersion solutions following sample removal after different immersion times: (a) DI-PBS-4.0 in 25/75% dioxane/water (v/v); (b) DI-HTMA-4.0 in 25/75% MeCN/water; (c) SP-PBS-3.4 in 25/75% dioxane/water (v/v).

5.3 Powder X-ray diffraction studies

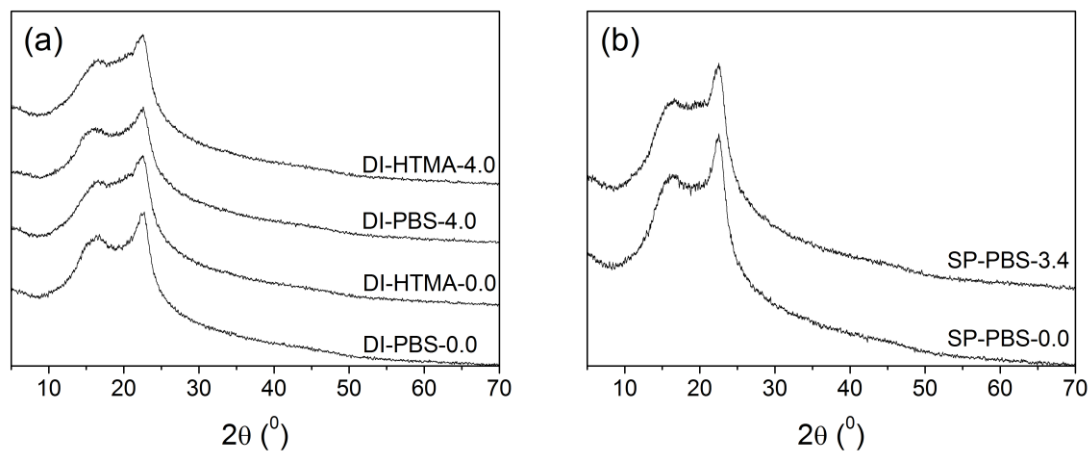


Figure S5. Powder X-ray diffractograms for (a) DI-PBS-0.0, DI-HTMA-0.0, DI-PBS-4.0 and DI-HTMA-4.0 and (b) SP-PBS-0.0 and SP-PBS-3.4 in the range $2\theta = 5-70^\circ$.

5.4 Solid-state nuclear magnetic resonance (NMR)

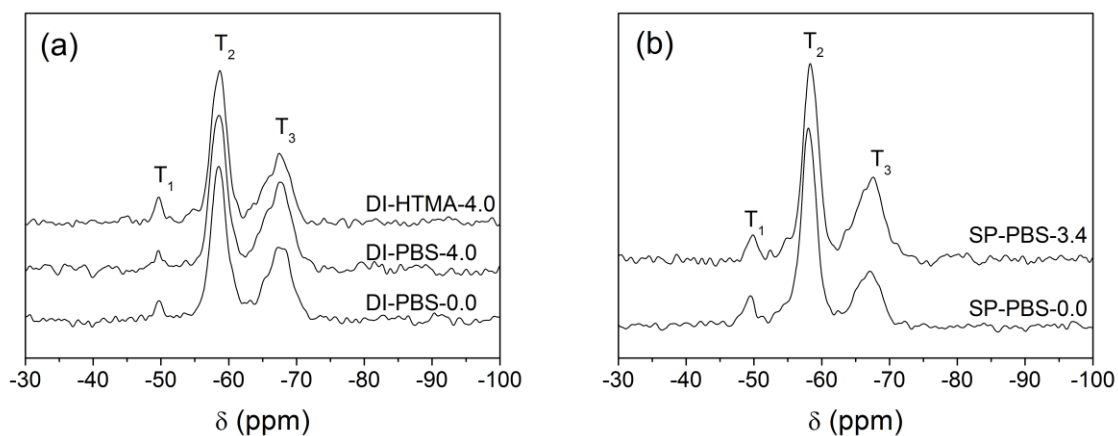


Figure S6. ^{29}Si solid-state MAS NMR spectra for (a) DI-PBS-0.0, DI-PBS-4.0 and SI-HTMA-4.0 and (b) SP-PBS-0.0 and SP-PBS-3.4.

Table S1: ^{29}Si MAS NMR chemical shifts (ppm vs TMS), population of different T_n species (%), T_n species ratios, and degree of condensation, C (%) of CPE-di-ureasils.

Sample	T_1 (%)	T_2 (%)	T_3 (%)	$T_1: T_2: T_3$	C (%) ^a
SP-PBS-0	-49.8 (7.5)	-58.4 (63.6)	-66.8 (28.8)	1: 8.5: 3.8	73.76
SP-PBS-3.4	-49.4 (4.4)	-58.1 (55.1)	-66.8 (40.5)	1: 12.5: 9.2	78.68
DI- PBS-0	-49.7 (3.4)	-58.6 (55.0)	-67.4 (41.6)	1: 16.2: 12.2	79.41
DI- PBS-4.0	-49.7 (3.0)	-58.5 (51.7)	-67.2 (45.3)	1: 17.2: 15.1	80.75
DI- HTMA-4.0	-49.6 (5.2)	-58.7 (55.3)	-67.4 (39.4)	1: 10.6: 7.6	78.07

^a $C = 1/3(\%T_1 + 2\%T_2 + 3\%T_3)$ ¹⁰

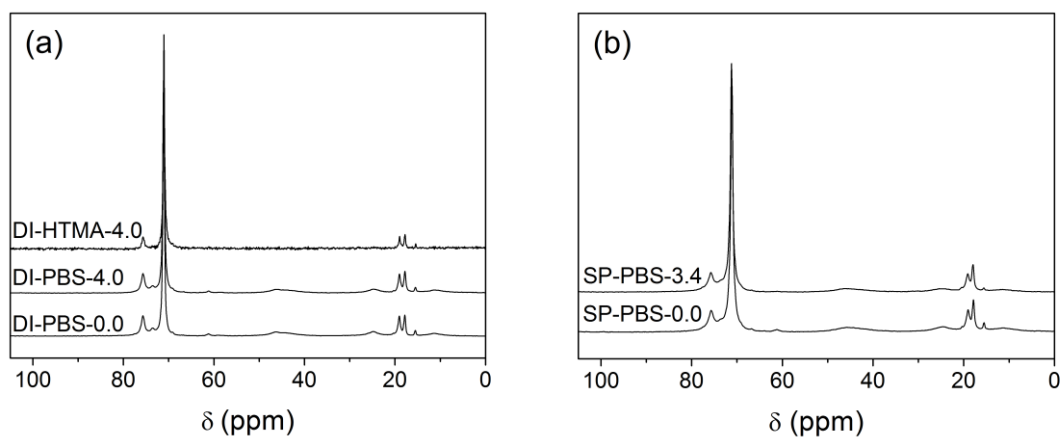


Figure S7. ^{13}C solid-state CP/MAS NMR spectra for (a) DI-PBS-0.0, DI-PBS-4.0 and DI-HTMA-4.0 and (b) SP-PBS-0.0 and SP-PBS-3.4.

5.5 Fourier transform infrared (FTIR) spectroscopy studies

Table S2. Results of Gaussian curve fitting of the ‘amide I’ band of CPE-di-ureasils prepared *via* Direct Insertion and Solvent Permeation methods, showing peak position, area and % contribution for each component resolved.

Sample	Peak position	Area (% contribution)	Peak position	Area (% contribution)	Peak position	Area (% contribution)
DI-PBS-0.0	1708	19.95 (26.3%)	1662	42.24 (55.6%)	1635	16.85 (18.1%)
DI-PBS-1.0	1708	19.90 (26.0%)	1663	41.72 (54.6%)	1635	15.92 (19.4%)
DI-PBS-2.0	1708	22.31 (28.8%)	1663	42.35 (54.7%)	1635	14.65 (16.5%)
DI-PBS-4.0	1707	21.19 (28.0%)	1662	40.74 (53.8%)	1635	14.29 (18.3%)
DI-HTMA-0	1709	20.11 (26.3%)	1663	43.52 (56.9%)	1636	16.32 (16.7%)
DI-HTMA-1.0	1711	19.67 (25.0%)	1664	45.85 (58.3%)	1636	14.93 (16.7%)
DI-HTMA-2.0	1709	19.91 (25.2%)	1664	42.87 (54.2%)	1636	15.91 (20.6%)
DI-HTMA-4.0	1708	21.43 (26.6%)	1663	41.81 (52.0%)	1635	14.38 (21.4%)
SP-PBS-0.0	1696	34.53 (41.2%)	1662	32.36 (38.6%)	1635	13.73 (20.1%)
SP-PBS-0.7	1701	24.7 (32.0%)	1662	38.19 (49.5%)	1636	13.86 (18.5%)
SP-PBS-2.0	1705	16.83 (23.1%)	1662	41.47 (56.8%)	1636	12.79 (20.1%)
SP-PBS-3.4	1701	23.05 (30.4%)	1662	38.19 (48.7%)	1635	14.84 (21.0%)

5.6 Steady-state photoluminescence (PL) studies

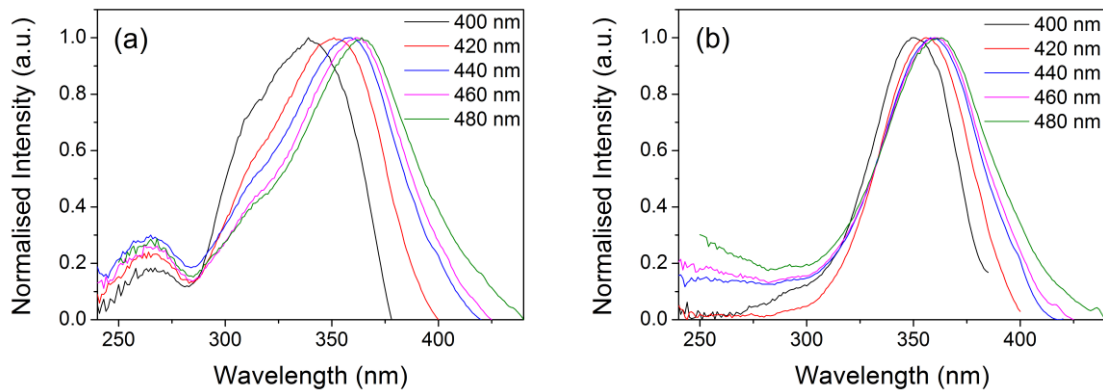


Figure S8. PL excitation spectra ($\lambda_{em} = 400, 420, 440, 460$ and 480 nm) for (a) DI-PBS-0.0 and (b) SP-PBS-0.0.

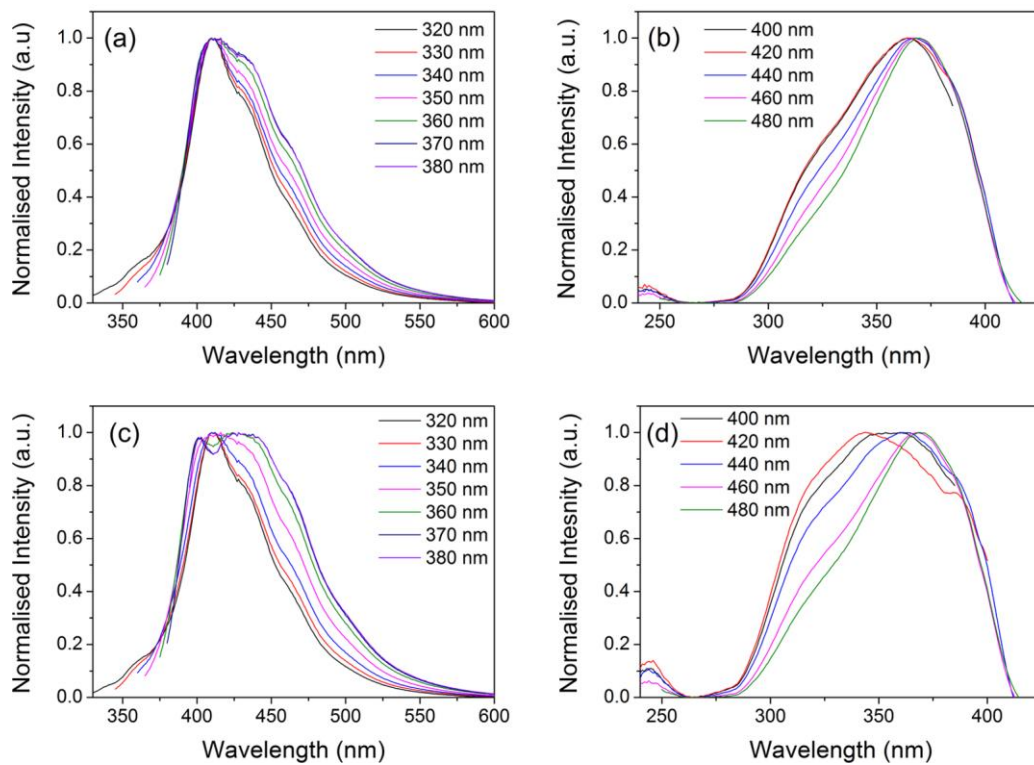


Figure S9. (a) PL spectra ($\lambda_{ex} = 320, 330, 340, 350, 360, 370$ and 380 nm) of DI-PBS-2.0, (b) PL excitation spectra ($\lambda_{em} = 400, 420, 440, 460$ and 480 nm) of DI-PBS-2.0, (c) PL spectra ($\lambda_{ex} = 320, 330, 340, 350, 360, 370$ and 380 nm) of DI-PBS-4.0, (d) PL excitation spectra ($\lambda_{em} = 400, 420, 440, 460$ and 480 nm) of DI-PBS-4.0.

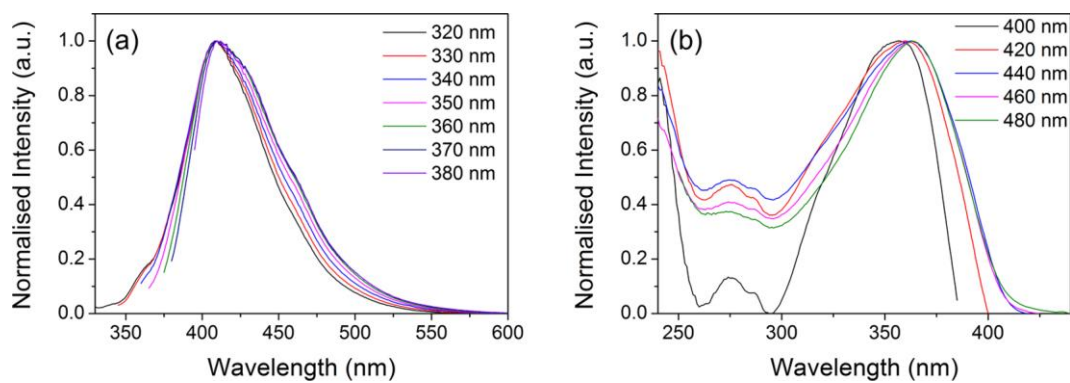


Figure S10. (a) PL spectra ($\lambda_{\text{ex}} = 320, 330, 340, 350, 360, 370$ and 380 nm) of SP-PBS-3.4 and (b) PL excitation spectra ($\lambda_{\text{em}} = 400, 420, 440, 460$ and 480 nm) of SP-PBS-3.4.

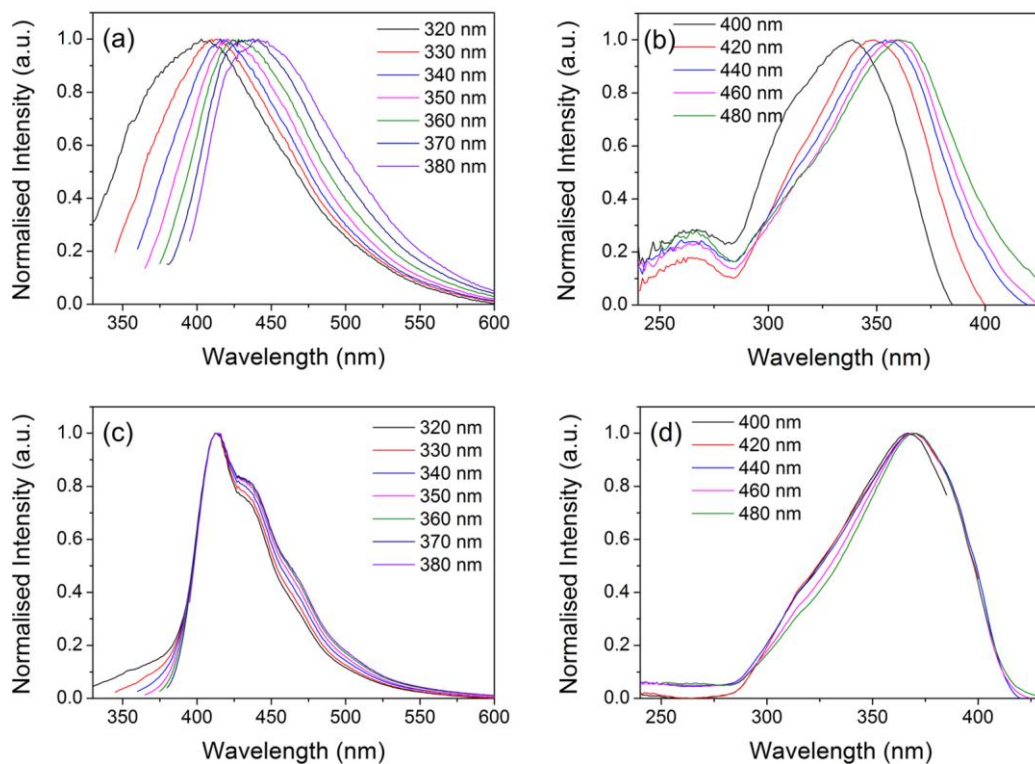


Figure S11. (a) PL spectra ($\lambda_{\text{ex}} = 320, 330, 340, 350, 360, 370$ and 380 nm) of DI-HTMA-1.0, (b) PL excitation spectra ($\lambda_{\text{em}} = 400, 420, 440, 460$ and 480 nm) of DI-HTMA-1.0, (c) PL spectra ($\lambda_{\text{ex}} = 320, 330, 340, 350, 360, 370$ and 380 nm) of DI-HTMA-2.0 and (d) PL excitation spectra ($\lambda_{\text{em}} = 400, 420, 440, 460$ and 480 nm) of DI-HTMA-2.0.

5.7 Picosecond (ps) time-correlated single photon counting (TC-SPC) studies

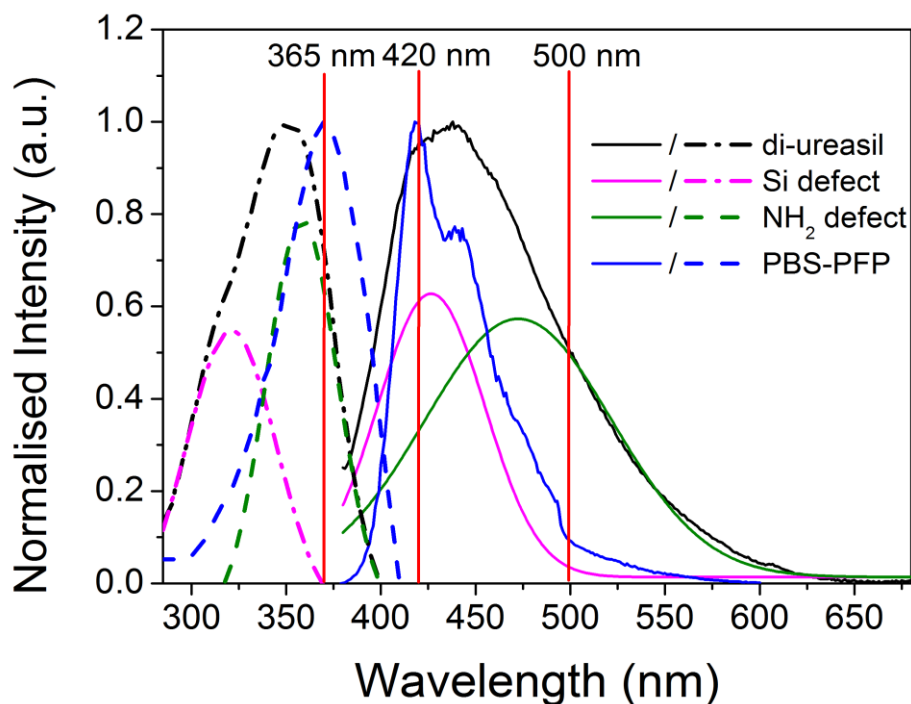


Figure S12. PL ($\lambda_{\text{ex}}=365$ nm) (solid lines) and excitation ($\lambda_{\text{em}}=420$ nm) (dashed lines) spectra for PBS-PFP in 25:75 % v/v 1,4-dioxane/water (blue) and DI-PBS-0 (black) showing the Gaussian peak fits for the two components that give rise to the di-ureasil emission and excitation spectra. These components are attributed to oxygen-related defects in the siliceous network (pink) and photoinduced proton transfer between NH₂ groups (dark green) respectively.

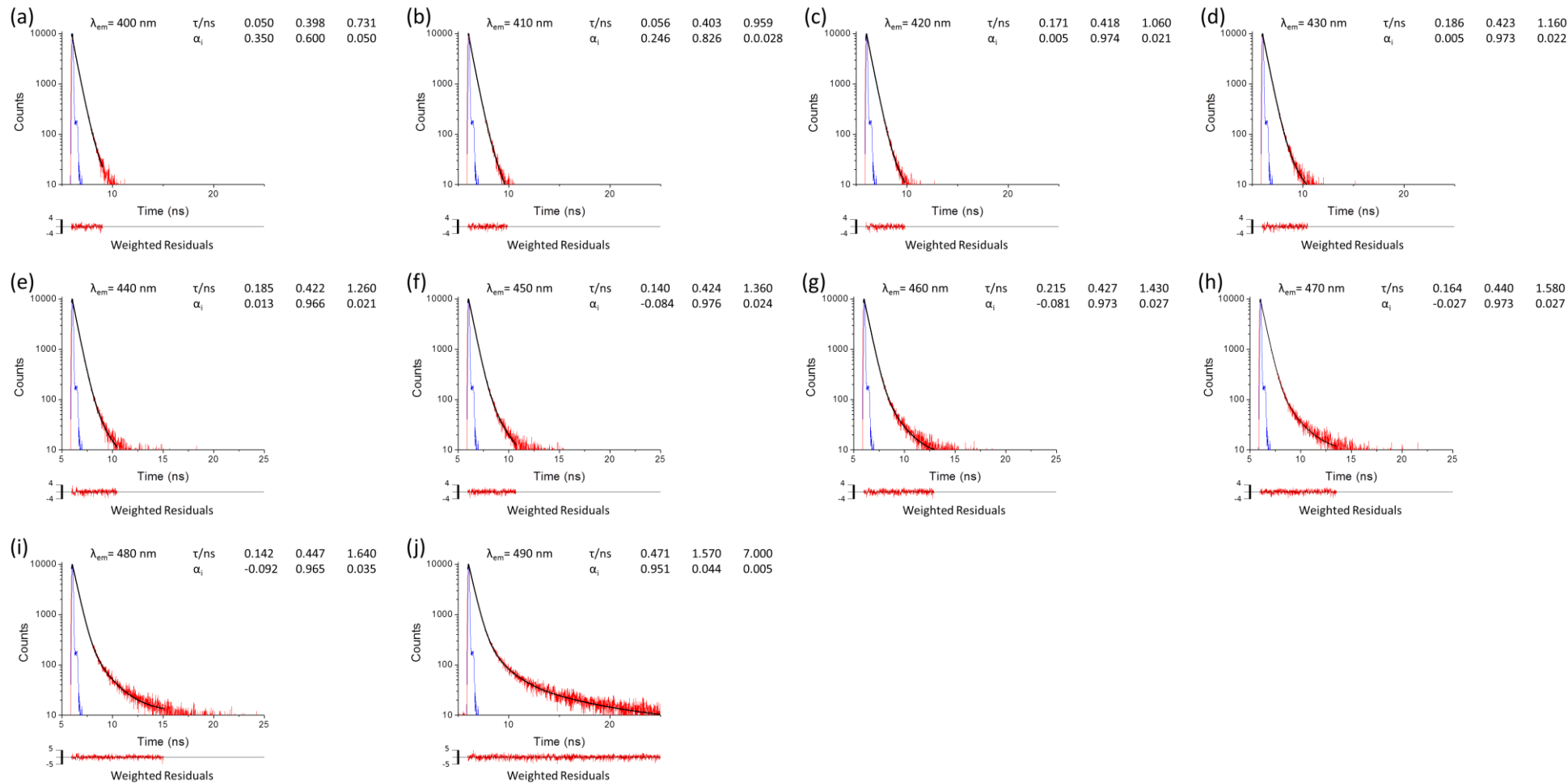


Figure S13. PL emission decay curves (solid red lines) and fits (solid black lines) for DI-PBS-1.0 as a function of emission wavelength (a) $\lambda_{em} = 400$ nm, (b) $\lambda_{em} = 410$ nm, (c) $\lambda_{em} = 420$ nm, (d) $\lambda_{em} = 430$ nm, (e) $\lambda_{em} = 440$ nm, (f) $\lambda_{em} = 450$ nm, (g) $\lambda_{em} = 460$ nm, (h) $\lambda_{em} = 470$ nm, (i) $\lambda_{em} = 480$ nm, (j) $\lambda_{em} = 490$ nm and (k) $\lambda_{em} = 500$ nm. The fitted decay times (τ_i), pre-exponentials (α_i), fits, weighted residuals and instrument response function (solid blue line) are also shown.

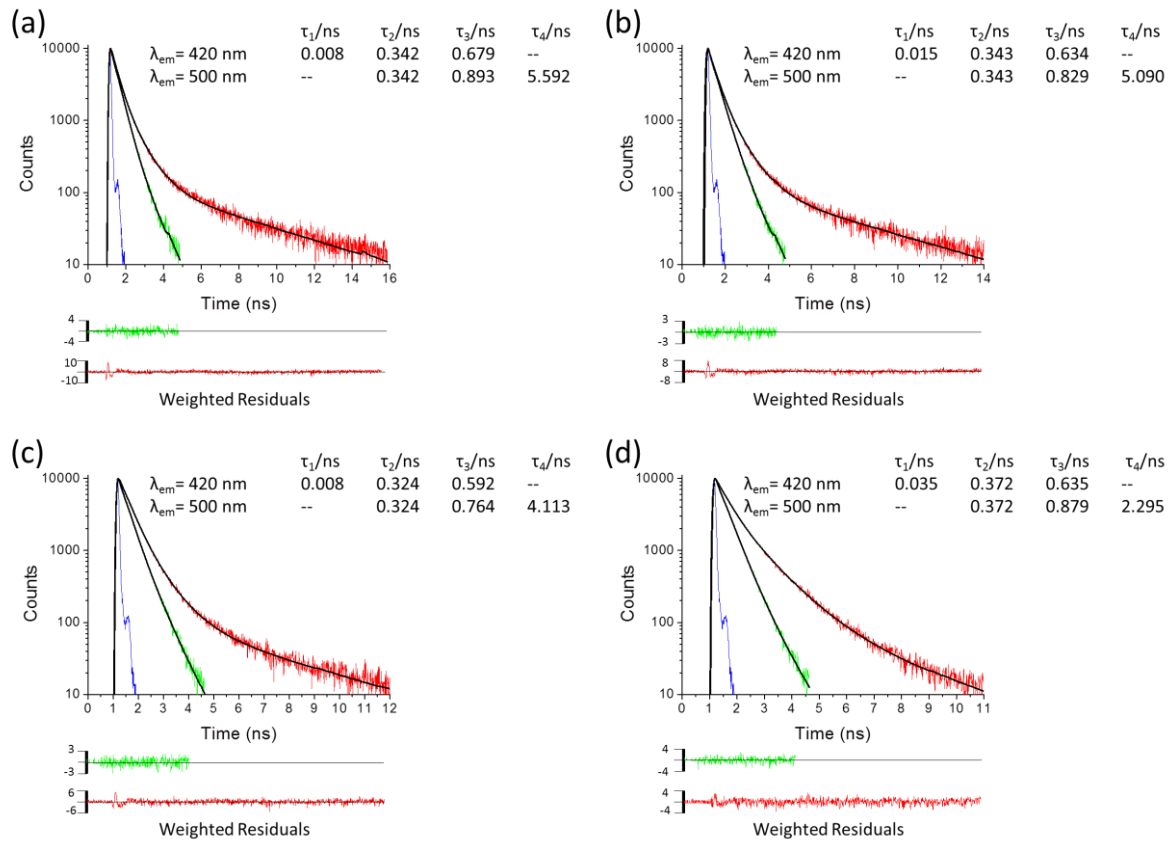


Figure S14. PL emission decay curves (solid green lines - $\lambda_{em}=420 \text{ nm}$, solid red lines - $\lambda_{em}=500 \text{ nm}$) and fits (solid black lines) for (a) DI-PBS-1.0, (b) DI-PBS-2.0, (c) DI-PBS-4.0 and (d) DI-PBS-8.0. The fitted decay times (τ_i), (α_i), fits, weighted residuals and instrument response function (solid blue line) are also shown.

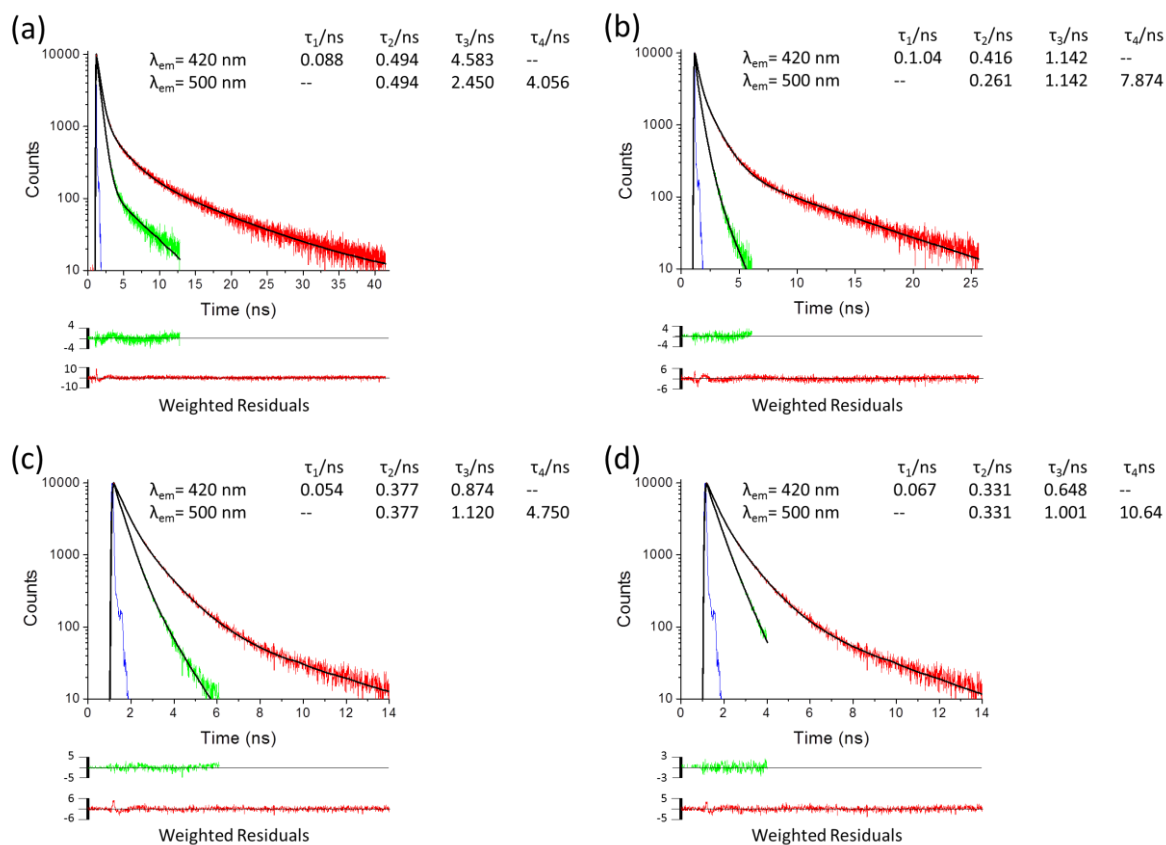


Figure S15. PL emission decay curves (solid green lines - $\lambda_{em}=420$ nm, solid red lines - $\lambda_{em}=500$ nm) and fits (solid black lines) for (a) DI-HTMA-1.0, (b) DI-HTMA-2.0, (c) DI-HTMA-4.0 and (d) DI-HTMA-8.0. The fitted decay times (τ_i), (α_i), fits, weighted residuals and instrument response function (solid blue line) are also shown.

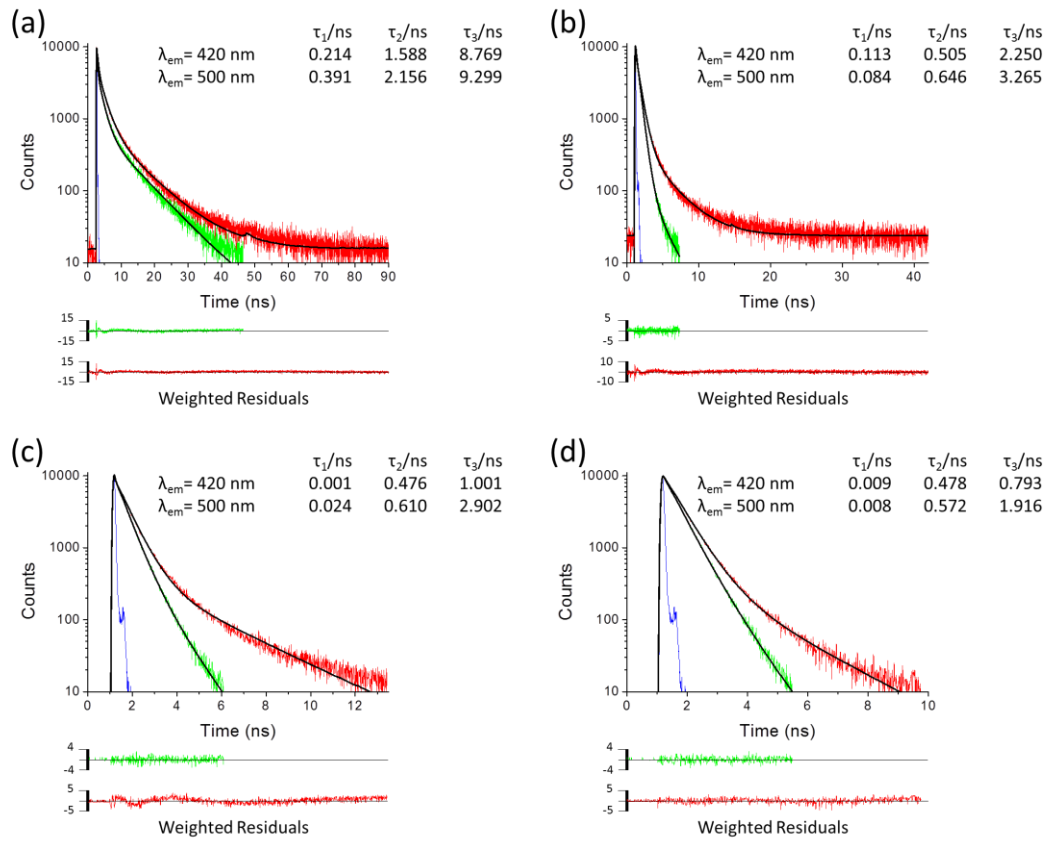


Figure S16. PL emission decay curves (solid green lines - $\lambda_{em}=420\text{ nm}$, solid red lines - $\lambda_{em}=500\text{ nm}$) and fits (solid black lines) for (a) SP-PBS-1.0, (b) SP-PBS-2.0, (c) SP-PBS-4.0 and (d) SP-PBS-8.0. The fitted decay times (τ_i), (α_i), fits, weighted residuals and instrument response function (solid blue line) are also shown.

Table S3. Decay times (τ_i), pre-exponential coefficients (α_i), fractional contribution (f_i) and chi squared (χ^2) values resulting from individual fits of the photoluminescence decays ($\lambda_{\text{ex}} = 365$ nm) of PBS-DI-1.0 at different emission wavelengths ($\lambda_{\text{em}} = 400 - 500$ nm).

λ_{em} (nm)	τ_1 (ns)	τ_2 (ns)	τ_3 (ns)	τ_4 (ns)	α_1	α_2	α_3	α_4	f_1	f_2	f_3	f_4	χ^2
400	0.050 ±0.008	0.398 ±0.010	0.731 ±0.250		0.350 ±0.002	0.600 ±0.001	0.050 ±0.0002		0.059 ±0.010	0.815 ±0.044	0.126 ±0.043		1.13
410	0.056 ±0.013	0.403 ±0.007	0.959 ±0.081		0.146 ±0.003	0.826 ±0.001	0.028 ±0.0002		0.022 ±0.005	0.904 ±0.023	0.074 ±0.007		1.15
420	0.171 ±0.004	0.418 ±0.001	1.060 ±0.054		0.005 ±0.001	0.974 ±0.001	0.021 ±0.0001		0.002 ±0.002	0.946 ±0.007	0.052 ±0.003		1.13
430	0.186 ±0.012	0.423 ±0.009	1.160 ±0.130		0.005 ±0.001	0.973 ±0.001	0.022 ±0.0001		0.002 ±0.003	0.940 ±0.030	0.058 ±0.007		1.22
440	0.185 ±0.009	0.422 ±0.008	1.260 ±0.150		0.013 ±0.001	0.966 ±0.001	0.021 ±0.0001		0.005 ±0.003	0.933 ±0.027	0.062 ±0.008		1.18
450	0.140 ±0.038	0.424 ±0.003	1.360 ±0.032		-0.084 ±0.001	0.976 ±0.001	0.024 ±0.0001		-0.027 ±0.008	0.952 ±0.013	0.075 ±0.002		1.01
460	0.215 ±0.057	0.427 ±0.006	1.430 ±0.055		-0.081 ±0.001	0.973 ±0.001	0.027 ±0.0001		-0.040 ±0.011	0.952 ±0.023	0.088 ±0.004		1.12
470	0.164 ±0.089	0.440 ±0.003	1.580 ±0.026		-0.027 ±0.001	0.973 ±0.001	0.027 ±0.0001		-0.009 ±0.006	0.917 ±0.011	0.092 ±0.002		1.05
480	0.142 ±0.034	0.447 ±0.004	1.640 ±0.035		-0.092 ±0.001	0.965 ±0.001	0.035 ±0.0001		-0.028 ±0.007	0.908 ±0.013	0.120 ±0.003		1.10
490		0.471 ±0.003	1.570 ±0.018	7.00 ±0.640		0.951 ±0.0003	0.044 ±0.0001	0.005 ±0.001		0.811 ±0.014	0.126 ±0.015	0.063 ±0.006	1.05
500		0.481 ±0.004	1.590 ±0.074	8.09 ±0.790		0.927 ±0.0004	0.066 ±0.0001	0.007 ±0.001		0.735 ±0.011	0.173 ±0.009	0.092 ±0.092	1.08

Table S4. Decay times (τ_i), pre-exponential coefficients (α_i), fractional contribution (f_i) and chi squared (χ^2) values resulting from Global analysis of the photoluminescence decays ($\lambda_{\text{ex}} = 365$ nm) of DI-HTMA- x at different emission wavelengths ($\lambda_{\text{em}} = 420$ and 500 nm).

Sample	τ_1 (ns)	τ_2 (ns)	τ_3 (ns)	α_1	α_2	α_3	f_1	f_2	f_3	χ^2
$\lambda_{\text{em}} = 420$ nm										
PFP-HTMA solution	0.069 \pm 0.004	0.446 \pm 0.004	0.949 \pm 0.010	0.465 \pm 0.021	0.427 \pm 0.010	0.108 \pm 0.003	0.099 \pm 0.007	0.586 \pm 0.012	0.315 \pm 0.008	1.04
DI-HTMA-0.0	0.453 \pm 0.007	2.459 \pm 0.022	9.890 \pm 0.069	0.744 \pm 0.014	0.208 \pm 0.004	0.047 \pm 0.001	0.256 \pm 0.006	0.389 \pm 0.008	0.356 \pm 0.007	1.51
DI-HTMA-1.0	0.088 \pm 0.008	0.494 \pm 0.004	4.583 \pm 0.138	0.340 \pm 0.017	0.649 \pm 0.013	0.011 \pm 0.001	0.074 \pm 0.008	0.795 \pm 0.015	0.131 \pm 0.006	1.28
DI-HTMA-2.0	0.104 \pm 0.003	0.416 \pm 0.004	1.142 \pm 0.052	0.619 \pm 0.017	0.353 \pm 0.014	0.028 \pm 0.001	0.264 \pm 0.011	0.604 \pm 0.027	0.132 \pm 0.007	1.07
DI-HTMA-4.0	0.054 \pm 0.005	0.377 \pm 0.003	0.874 \pm 0.024	0.338 \pm 0.016	0.569 \pm 0.010	0.094 \pm 0.002	0.058 \pm 0.006	0.682 \pm 0.012	0.260 \pm 0.009	1.21
DI-HTMA-8.0	0.067 \pm 0.006	0.331 \pm 0.004	0.648 \pm 0.005	0.248 \pm 0.016	0.436 \pm 0.009	0.316 \pm 0.006	0.046 \pm 0.005	0.395 \pm 0.008	0.559 \pm 0.009	0.85
$\lambda_{\text{em}} = 500$ nm										
DI-HTMA-0.0	0.453 \pm 0.016	3.019 \pm 0.029	11.22 \pm 0.069	0.646 \pm 0.027	0.285 \pm 0.008	0.069 \pm 0.002	0.152 \pm 0.008	0.445 \pm 0.011	0.403 \pm 0.009	1.67
DI-HTMA-1.0	0.494 \pm 0.008	2.450 \pm 0.028	10.64 \pm 0.136	0.716 \pm 0.018	0.084 \pm 0.013	0.200 \pm 0.001	0.132 \pm 0.004	0.077 \pm 0.002	0.792 \pm 0.013	1.33
DI-HTMA-2.0	0.261 \pm 0.008	1.142 \pm 0.007	7.874 \pm 0.138	0.666 \pm 0.026	0.313 \pm 0.014	0.022 \pm 0.001	0.248 \pm 0.012	0.510 \pm 0.010	0.242 \pm 0.007	1.27
DI-HTMA-4.0	0.377 \pm 0.010	1.120 \pm 0.006	4.750 \pm 0.059	0.660 \pm 0.025	0.325 \pm 0.010	0.015 \pm 0.002	0.364 \pm 0.016	0.533 \pm 0.014	0.103 \pm 0.006	1.35
DI-HTMA-8.0	0.331 \pm 0.007	1.001 \pm 0.007	4.056 \pm 0.194	0.569 \pm 0.026	0.411 \pm 0.009	0.020 \pm 0.006	0.277 \pm 0.009	0.604 \pm 0.010	0.119 \pm 0.007	1.06

Table S5. Decay times (τ_i), pre-exponential coefficients (α_i), fractional contribution (f_i) and chi squared (χ^2) values resulting from Global analysis of the photoluminescence decays ($\lambda_{\text{ex}} = 365$ nm) of SP-PBS- x at different emission wavelengths ($\lambda_{\text{em}} = 420$ and 500 nm).

Sample	τ_1 (ns)	τ_2 (ns)	τ_3 (ns)	α_1	α_2	α_3	f_1	f_2	f_3	χ^2
$\lambda_{\text{em}} = 420$ nm										
PBS-PFP solution	0.076 \pm 0.004	0.347 \pm 0.021	0.817 \pm 0.015	0.483 \pm 0.003	0.380 \pm 0.001	0.138 \pm 0.001	0.135 \pm 0.008	0.486 \pm 0.033	0.379 \pm 0.015	1.03
SP-PBS-0.0	0.214 \pm 0.003	1.588 \pm 0.023	8.769 \pm 0.092	0.628 \pm 0.095	0.315 \pm 0.039	0.057 \pm 0.007	0.119 \pm 0.017	0.442 \pm 0.048	0.439 \pm 0.043	2.52
SP-PBS-0.7	0.113 \pm 0.009	0.505 \pm 0.003	2.250 \pm 0.696	0.280 \pm 0.018	0.707 \pm 0.014	0.013 \pm 0.001	0.076 \pm 0.008	0.856 \pm 0.022	0.068 \pm 0.021	1.09
SP-PBS-2.0	0.001 \pm	0.476 \pm	1.001 \pm	0.781 \pm	0.194 \pm	0.025 \pm	0.007 \pm	0.779 \pm	0.214 \pm	0.93
SP-PBS-7.0	0.009 \pm 0.001	0.478 \pm 0.003	0.793 \pm 0.010	0.625 \pm 0.037	0.309 \pm 0.010	0.066 \pm 0.003	0.027 \pm 0.004	0.718 \pm 0.011	0.255 \pm 0.007	0.95
$\lambda_{\text{em}} = 500$ nm										
SP-PBS-0.0	0.391 \pm 0.023	2.156 \pm 0.039	9.299 \pm 0.145	0.560 \pm 0.029	0.370 \pm 0.011	0.070 \pm 0.002	0.131 \pm 0.010	0.477 \pm 0.014	0.392 \pm 0.012	1.53
SP-PBS-0.7	0.084 \pm 0.005	0.646 \pm 0.008	3.265 \pm 0.046	0.467 \pm 0.061	0.503 \pm 0.030	0.029 \pm 0.002	0.085 \pm 0.012	0.707 \pm 0.023	0.208 \pm 0.009	1.43
SP-PBS-2.0	0.024 \pm 0.003	0.610 \pm 0.006	2.902 \pm 0.051	0.588 \pm 0.045	0.391 \pm 0.016	0.020 \pm 0.001	0.045 \pm 0.006	0.768 \pm 0.015	0.187 \pm 0.007	1.67
SP-PBS-7.0	0.008 \pm 0.002	0.572 \pm 0.004	1.916 \pm 0.026	0.632 \pm 0.061	0.349 \pm 0.019	0.019 \pm 0.001	0.021 \pm 0.005	0.829 \pm 0.015	0.150 \pm 0.005	1.29

6. References

1. H. D. Burrows, V. M. M. Lobo, J. Pina, M. L. Ramos, J. S. de Melo, A. J. M. Valente, M. J. Tapia, S. Pradhan and U. Scherf, *Macromolecules*, 2004, **37**, 7425-7427.
2. A. Garcia, J. Z. Brzezinski and T.-Q. Nguyen, *J. Phys. Chem. C*, 2009, **113**, 2950-2954.
3. R. Yang, H. Wu, Y. Cao and G. C. Bazan, *J. Am. Chem. Soc.*, 2006, **128**, 14422-14423.
4. V. de Zea Bermudez, L. D. Carlos and L. Alcácer, *Chem. Mater.*, 1999, **11**, 569-580.
5. L. D. Carlos, V. de Zea Bermudez, R. A. S. Ferreira, L. Marques and M. Assunção, *Chem. Mater.*, 1999, **11**, 581-588.
6. L. D. Carlos, R. A. S. Ferreira, V. de Zea Bermudez and S. J. L. Ribeiro, *Adv. Funct. Mater.*, 2001, **11**, 111-115.
7. E. Gratton, J. Beechem, Globals WE (software), Laboratory for Fluorescence Dynamics, University of California, Irvine, CA 2004.
8. T.-S. Ahn, R. O. Al-Kaysi, A. M. Müller, K. M. Wentz and C. J. Bardeen, *Rev. Sci. Instrum.*, 2007, **78**, 086105.
9. J. C. de Mello, H. F. Wittmann and R. H. Friend, *Adv. Mater.*, 1997, **9**, 230-232.
10. P. P. Lima, R. A. S. Ferreira, S. A. Júnior, O. L. Malta and L. D. Carlos, *J. Photochem. Photobiol. A*, 2009, **201**, 214-221.